Localization and Dephasing Effects in a Time-Dependent Anderson Hamiltonian

D. A. Evensky, R. T. Scalettar, and P. G. Wolynes*

School of Chemical Sciences, University of Illinois, Urbana, Illinois 61801 *(Received: July 5, 1989; In Final Form: October 16, 1989)*

In this paper we study a generalization of the Anderson model of localization which includes time-dependent on-site randomness to elucidate the interplay between dephasing and localization. We find, in agreement with recent approximate treatments, that the inclusion of dephasing initially increases diffusion away from a localized state but then eventually inhibits spatial spreading of the wave function. For a delocalized state, dephasing can either monotonically decrease the diffusion rate or produce a weak maximum.

1. Introduction

The peculiarities of charge and exciton transport in solids have intrigued scientists for many decades. Even in the 1920s, students of chemical physics were aware of the perplexing nature of these problems and proposed experimental and theoretical approaches.[1] In fact, these are highly quantum mechanical phenomena relying on the precise tuning of energy levels. That essential physical insight was provided by Peierls[2] and Wilson[3] for perfect crystals and by Anderson[4] for disordered systems. The seminal experimental work using this insight was done by Drickamer[5] who showed that pressure tuning could effect a metal–insulator transition in crystalline materials. Pressure (stress) tuning features prominently in the experimental work on electron transport in disordered materials as well.[6] It has also been used by Drickamer in his pioneering study of exciton transport.[7] Since conduction and electron transport rely on tuning of energy levels, it is obviously of interest to examine the influence of dynamic fluctuations in energy levels on these processes. In this contribution we report simulations addressing that issue in the context of disordered systems.

The Anderson model of localization is one of the simplest descriptions of the physics of disordered systems. It describes the transition, with increasing disorder, from the usual extended Bloch states charcteristic of periodic crystalline potentials to states which are spatially localized. The Anderson model has been extensively studied by a variety of analytical and numerical techniques.[8] It is now widely believed that any amount of disorder in one and two dimensions results in localization of the eigenfunctions. In three dimensions, there is a critical amount of disorder required for the delocalized states to disappear. Near the edge of the band, where the density of states is least, localization appears first. A Mott mobility edge separates these states from extended ones closer to the band center.

Fluctuations in the energy levels caused, for example, by the interaction of the electrons with phonon or exciton modes can destroy the sharpness of this transition and lead to the incoherent transport phenomena seen in many experiments. Because of the importance of these interactions, a variety of approximate analytic approaches to quantum transport with fluctuating energy levels have been taken.[9-11] With few exceptions, these treatments do not claim to describe all regimes of transport in a uniform way. One of the most direct unified approaches is due to Logan and Wolynes[12] who have recently studied the effect of dynamical fluctuations on localization by an approximate theory. Following Abou-Chacra, Anderson, and Thouless[13] a self-consistent equation is written for the imaginary part of the self-energy Δ_i of an electronic state localized at site i. A complicated integral equation results from the self-consistency requirement on the probability distribution of Δ_i. This is simplified by demanding only that the most probable value of Δ be self-consistently determined. The resulting condition now takes the form of an algebraic equation which allows the mobility edge to be studied from either side of the localization–delocalization transition.

This approach lends itself well to the inclusion of a phenomenological dephasing rate η which reflects the dynamical fluctuations. Allowing for this interplay between the static and time-dependent randomness leads in a natural way to the phenomenon of Mooij correlation[14]—the observation that weakly disordered metals with small residual resistivities have positive temperature coefficients of resistivity while for strongly disordered metals the situation is reversed and the resistivity initially decreases with increasing temperature. This latter case is in accordance with a physical picture which suggests that thermal fluctuations first assist isolated energy levels to come into resonance but then ultimately can inhibit motion when T is too high since excessively large time-dependent randomness again allows different levels only rarely to come into resonance. This large η regime is analogous to the phenomenon of Förster[15] transport for excitons where the diffusion constant falls as the inverse of the dephasing rate.

In this paper we consider the dynamics of a single particle interacting with a random space- and time-dependent field; i.e., we add to the usual site disordered Anderson model the feature that the random site energies are allowed to depend on time. As described above, we are particularly interested in determining how this time dependence affects the transport properties. We have used a classically fluctuating time-dependent randomness which has no correlations in time. This is an approach which is exact

(1) Oppenheimer, J. R. Letters to P. W. Bridgman, dated June 29, 1925 and September 5, 1925, and February 12, 1927, reproduced in: *Robert Oppenheimer: Letters and Recollections*; Smith, A. K., Weiner, C., Eds.; Harvard University Press: Cambridge, MA, 1980.
(2) Peierls, R. *Ann. Phys.* **1930**, *4*, 121.
(3) Wilson, A. H. *Proc. R. Soc.* **1932**, *138A*, 594. Wilson, A. H. *Proc. R. Soc.* **1935**, *151A*, 274.
(4) Anderson, P. W. *Phys. Rev.* **1958**, *109*, 1492.
(5) Riggleman, B. M.; Drickamer, H. G. *J. Chem. Phys.* **1962**, *37*, 446. Riggleman, B. M.; Drickamer, H. G. *J. Chem. Phys.* **1963**, *38*, 2721.
(6) Rosenbaum, T. F.; Andres, K.; Thomas, G. A. *Solid State Commun.* **1980**, *35*, 663. Rosenbaum, T. F.; Andres, K.; Thomas, G. A.; Bhatt, R. N. *Phys. Rev. Lett.* **1980**, *45*, 1723. Rosenbaum, T. F.; Andres, K.; Thomas, G. A.; Lee, P. A. *Phys. Rev. Lett.* **1981**, *46*, 568. Rosenbaum, T. F.; Milligan, R. F.; Paalanen, M. A.; Thomas, G. A.; Bhatt, R. N.; Lin, W. *Phys. Rev.* **1983**, *B27*, 7509.
(7) Bieg, K. W.; Drickamer, H. G. *J. Chem. Phys.* **1977**, *66*, 1437.
(8) For a review, see: Lee, P. A.; Ramakrishnan, T. V. *Rev. Mod. Phys.* **1987**, *57*, 287.
(9) Jonson, M.; Girvin, S. M. *Phys. Rev. Lett.* **1979**, *43*, 1447. Jonson, M.; Girvin, S. M. *Phys. Rev.* **1980**, *B22*, 3583.
(10) Kenkre, V. M.; Knox, R. S. *Phys. Rev.* **1974**, *B9*, 5279. Klafter, J.; Silbey, R. *Phys. Rev. Lett.* **1980**, *44*, 55. Loring, R. F.; Mukamel, S. *Phys. Rev.* **1986**, *B33*, 7708.
(11) Nagaoka, Y., Fukuyama, H., Eds. *Anderson Localization*; Springer: Berlin, 1982. Kramer, B., Bergmann, G., Bruynseraede, Y., Eds. *Localization, Interaction, and Quantum Transport*; Springer: Berlin, 1985. Mott, N. F.; Kaveh, M. *Adv. Phys.* **1985**, *34*, 329.
(12) Logan, D. E.; Wolynes, P. G. *Phys. Rev.* **1987**, *B36*, 4135.
(13) Abou-Chacra, R.; Anderson, P. W.; Thouless, D. J. *J. Phys.* **1973**, *C6*, 1734.
(14) Mooij, J. H. *Phys. Status Solidi* **1973**, *A17*, 521.
(15) Förster, Th. *Ann. Phys. (N.Y.)* **1948**, *2*, 55.

0022-3654/90/2094-1149$02.50/0

only in the limit of high temperature. It might nevertheless represent an adequate description for example of the physics of excitons in molecular crystals. A more realistic approach would determine the field in which the electron moves in some self-consistent manner from the electron wave function itself. We will comment further on some possible approaches later.

In section 2 we will describe in more detail the model we are considering. Section 3 will detail our numerical technique for evolving the Schroedinger equation using the "Trotter approximation" to construct the time evolution operator. Section 4 contains our results for the mobility edge in the case $\eta = 0$ and a discussion of the effects of nonzero dephasing. Section 5 is a brief conclusion.

2. The Model

We study the Hamiltonian

$$\hat{H} = -V\sum_{\langle i,j\rangle}(c_i^\dagger c_j + c_j^\dagger c_i) + \sum_i(\epsilon_i + \phi_i(t))n_i \qquad (1)$$

where the ϵ_i's and $\phi_i(t)$'s are drawn from independent Gaussian distributions such that

$$\langle \epsilon_i \epsilon_j \rangle = \frac{\sigma^2}{2}\delta_{ij}$$

$$\langle \phi(t)\ \phi_j(t')\rangle = \sigma'^2\delta_{ij}\delta(t - t') \qquad (2)$$

The transfer matrix element V is nonzero between nearest-neighbor sites $\langle i,j\rangle$ on a three-dimensional cubic lattice. We set $V = 1$ to define the scale of energy. ϵ_i is a time-independent random on-site energy. This constitutes the usual Hamiltonian used to study the effect of randomness on localization, though the effect of topological disorder $V \rightarrow V_{ij}$ can also be included. We add a third on-site random but now *time-dependent* term $\phi_i(t)$ which will control the dephasing rate. For all the situations described in this paper $\phi_i(t)$ is decorrelated in both space and time; i.e., its evolution knows nothing about the electronic wave function. σ' is, of course, related to a dephasing rate by the standard formula

$$\eta = \int \langle \phi_i(0)\ \phi_i(t)\rangle\ \mathrm{d}t \qquad (3)$$

This is a good point at which to clarify our use of the term "dephasing rate". The distinction between "pure" dephasing and inelastic events which also destroy phase is basis dependent. In the original site basis the fluctuating field can only act to randomize the phase relations of sites and would be "pure" dephasing; in a plane wave basis or unperturbed eigenstate basis it would cause inelastic events. What is relevant for localization is the phase relations between sites, and hence anything contributing to this affects the transition. The "purity" of the dephasing is not significant in this context, although it may be in other contexts.

The choice of ϕ to be an autonomous field is essentially a high-temperature approximation. The temperature T will enter the calculation only through the choice of the dephasing rate. The site occupation probability will show no Boltzmann factor $e^{-\beta\epsilon_i}$ which preferentially occupies sites of low energy. We are currently investigating cases when time correlations in ϕ are present. This would be a more realistic model of, for example, the coupling of the electronic charge to some local phonon degrees of freedom. One approach is to determine the bosonic degrees of freedom $\phi_i(t)$ in a self-consistent way from the electronic wave function by including a force on ϕ determined by the expectation value of the Hamiltonian $\hat{H}$ in the electronic state $|\psi\rangle$ so as to conserve the total energy of the system. Sites with low energy ϵ_i will be more highly occupied since more energy, and hence more phase space, will then be available for the bosonic degrees of freedom. This is a reasonable approximation for cases when the electronic wave function is sharply peaked and has been used, for example, by Car and Parrinello[16] in studying the motion of electrons in a fluid. This approximation has been explored by Cline and Wolynes[17] in studies of two-level system dynamics and also by Miller.[18] In these papers various problems with this approach are discussed. The basic difficulty is that it inadequately treats cases when the quantum mechanical particle has many different possible wave functions which represent quite different configurations. Treating the state as a single linear combination is not adequate; a density matrix approach is more appropriate. The inclusion of detailed balance correctly is a delicate matter, and we will discuss it no further in this paper.

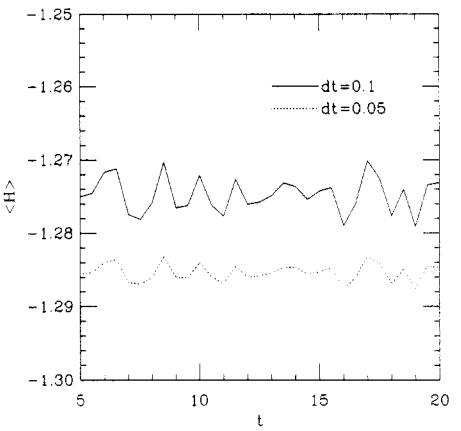

Figure 1. Plot of the mean energy, $\langle H\rangle$, vs t for a 20^3 lattice. The transfer matrix element $V = 1$, the static randomness width $\sigma = 1$; there is no dephasing ($\eta = 0$). The full curve is $\mathrm{d}t = 0.1$ and the dashed curve $\mathrm{d}t = 0.05$. Note that the numerical evolution keeps the mean energy constant to a high degree of accuracy.

3. Numerical Methods

In this section we will describe our numerical technique and also give some preliminary results to illustrate various features of our approach. We are interested in studying the time evolution of the wave function for a single electron propagating in a disordered medium. Rather than performing a standard numerical integration of the Schroedinger equation, we utilize an approach[19] suggested by Monte Carlo simulations of many-body systems.[20] We apply the operator $e^{-i\hat{H}t}$ to a wave function ψ by utilizing the Trotter approximation,[21]

$$e^{-i\hat{H}t} = e^{-i(\hat{H}_1+\hat{H}_2+\hat{H}_3)t} = [e^{-i(\hat{H}_1+\hat{H}_2+\hat{H}_3)\,\mathrm{d}t}]^P \qquad (4)$$

$$\approx [e^{-i\hat{H}_1\,\mathrm{d}t}e^{-i\hat{H}_2\,\mathrm{d}t}e^{-i\hat{H}_3\,\mathrm{d}t}]^P$$

Here $\hat{H}_1$, $\hat{H}_2$, and $\hat{H}_3$ are the various pieces of our Hamiltonian and $P = t/\mathrm{d}t$. Equation 4 is an approximation, of course, because the $\hat{H}_i$ do not commute with each other. However, the errors associated with such a decomposition[22] are of order $[\hat{H}_i, \hat{H}_j]$, i.e., $(\mathrm{d}t)^2\ E_iE_j$, where E_i and E_j are typical energy scales in $\hat{H}_i$ and $\hat{H}_j$. Although it is possible by such estimates to get an idea for the nature of the size of the approximations involved, in practice we simply choose $\mathrm{d}t$ small enough so that our results are unchanged at the level of a few percent. We have typically chosen to run with $\mathrm{d}t = 0.05$ or smaller.

There are two ways to deal with the exponential of the kinetic energy term in the Hamiltonian. The first is to employ fast Fourier transforms to convert from position representation, where the exponentiation of the site-diagonal terms is straightforward, to momentum space where the application of $e^{-i\hat{K}\,\mathrm{d}t}$ is most easily accomplished. The second is to employ a "checkerboard" or similar decomposition[20,23] of the kinetic energy into several pieces which

(16) Car, R.; Parrinello, M. In *Proceedings of the Eighteenth International Conference on the Physics of Semiconductors, Stockholm, 1986*; Engstrom, O., Ed.; World Scientific: Singapore, 1987; pp 1165–72.

(17) Cline, R. E.; Wolynes, P. G. *J. Chem. Phys.* **1987**, *86*, 3836.

(18) Makri, N.; Miller, W. H. *J. Chem. Phys.* **1987**, *87*, 5781.

(19) Feit, M. D.; Fleck, Jr., J. A.; Steiger, A. *J. Comput. Phys.* **1982**, *47*, 412. De Raedt, H. *Comp. Phys. Rep.* **1987**, *7*, 1.

(20) Scalapino, D. J.; Sugar, R. L. *Phys. Rev.* **1981**, *B24*, 4295.

(21) Trotter, H. F. *Proc. Am. Math. Soc.* **1959**, *10*, 545. Suzuki, M. *Comm. Math. Phys.* **1976**, *51*, 183. DeRaedt, H.; De Raedt, B. *Phys. Rev.* **1983**, *A28*, 3575.

(22) Fye, R. M. *Phys. Rev.* **1986**, *B33*, 6271. Fye, R. M.; Scalettar, R. T. *Phys. Rev.* **1987**, *B36*, 3833.

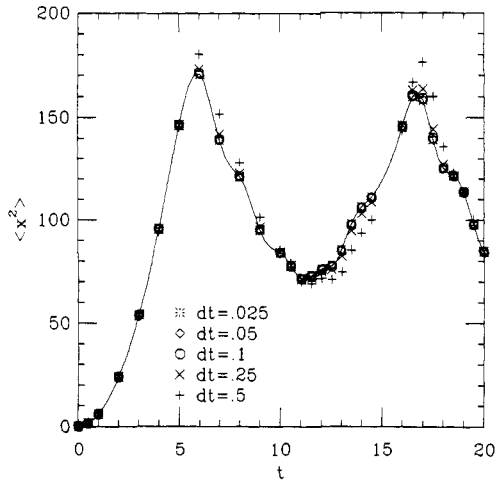

Figure 2. Plot of the expectation value of the square of the distance from the origin $\langle x^2 \rangle$ vs t for a 20^3 lattice with $V = 1$ and $\sigma = 0.0$. The solid curve consists of the analytical values and the symbols are the simulation values with dt's of 0.5, 0.25, 0.1, 0.05, and 0.025. The initial value of the wave function, $\psi(0)$ is δ_{i,i_0}, where i_0 is the initial site.

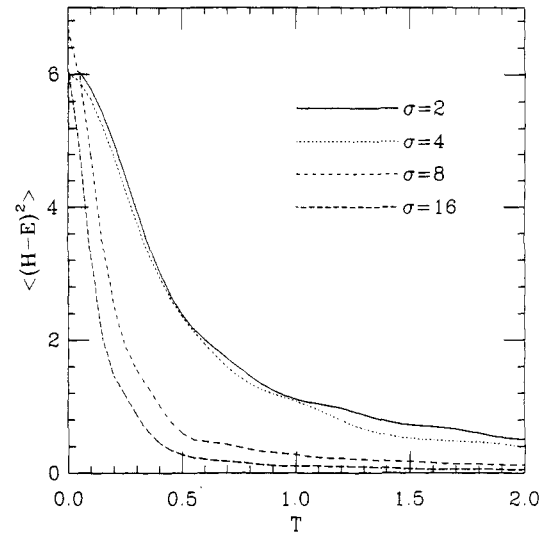

Figure 3. Plot of the square of the error of the projection $\langle \psi_E(T)|(H - E)^2|\psi_E(T)\rangle$ vs T for a 20^3 lattice with $V = 1$. E is the desired energy of the wavepacket and $\psi_E(T)$ is the wave function at time T. Projection errors for systems with static randomness widths σ of 2, 4, 8, and 16 are shown. The time step is 0.025 and the desired energy, E, is 0.0. The origin was selected from sampling initially with a broad state as described in the text.

are easily exponentiated. This introduces errors only at the same level as the initial division into kinetic and potential terms and hence is not a source of additional systematic effects. For problems with long-range transfer matrix elements, for example in the study of dipolar exciton propagation, the fast Fourier transform method would be the more efficient one. For short range hopping the checkerboard decomposition is somewhat more rapid and hence is employed here.

We show in Figure 1 a plot of $E = \langle \psi(t)|\hat{H}|\psi(t)\rangle$ as a function of time for $V = 1$, $\sigma = 1$, and $\sigma' = 0$. In such a case, when there is no dephasing, E should be independent of t. We see that the Trotter approximation has introduced fluctuations in E of the order of 1% for dt = 0.10 and 0.3% for dt = 0.05. Figure 1 also illustrates another important aspect of this technique for the time evolution of ψ, namely its stability property—errors tend to be random rather than cumulative.

A second measure of the effect of errors associated with the choice of finite dt is obtained by solving for the time evolution analytically in the case $\sigma = \sigma' = 0$ and comparing with results obtained using the checkerboard decomposition. In Figure 2 we show, as the full curve, exact, analytic values for the mean square displacement $\langle x^2 \rangle$ from the origin of a particle started from an initial wave function localized at the origin. A lattice of 20^3 sites was used. The different symbols show values for this quantity for various dt obtained from a simulation employing the checkerboard decomposition. (The fast Fourier transform technique would in this case give the exact results for all dt.) We see that for dt as large as 0.25 the systematic errors are small. Again, the stability of the algorithm is evident. The saturation of the mean square displacement as a function of time, and its subsequent oscillations, are associated with the wavepacket reaching the edge of the box and then interfering with itself on its return (we employ periodic boundary conditions here). For a box of side L, we see that such edge effects appear when the mean square displacement reaches roughly $(L/2)^2$. In our later studies of the diffusion constant (see below) we will have to cut off our simulation before such effects become important. Note finally that $\langle x^2 \rangle$ shows a ballistic motion, i.e., grows quadratically with t in the limit of no randomness. The inclusion of site disorder converts this growth to a linear, diffusive, one.

To study the physics of localization, it is convenient to have wave packets of well-defined energy. (This is necessary, for example, if we want to determine the location of the mobility edge for some set of parameters.) Of course, $\langle \hat{H} \rangle$ is not constant if $\sigma' \neq 0$, so we cannot strictly speak of a state of well-defined energy in that case. However, if the relaxation away from E associated with $\sigma' \neq 0$ is sufficiently slow, we may still sensibly imagine evolving a state of energy E even in the presence of nonzero time-dependent randomness.

We project out a wave packet of energy E and width Γ via the formula

$$|\psi_E(T)\rangle = \int_{-T}^{T} dt \exp\left(\frac{-t^2}{2\Gamma^2}\right) e^{iEt} e^{-i\hat{H}t} |\psi_0\rangle \qquad (5)$$

For $\Gamma = 0$ and $T \to \infty$, $|\psi_E(T)\rangle$ approaches an eigenstate of $\hat{H}$ of eigenvalue E, assuming that $|\psi_0\rangle$ is not orthogonal to such a state and assuming that E is the indeed chosen to be an eigenstate of $\hat{H}$. Since we in general will not know the eigenstates, we typically choose $\Gamma \approx 1/4$. For the systems of order 10^4 sites and bandwidth ≈ 20 that we study, this choice of Γ guarantees many eigenstates will lie within Γ of an arbitrarily chosen E. Additionally, for a finite Γ, $T \approx 1/\Gamma$ does not have to be excessively large.

A final technical point is the following: Since we will be studying diffusion, we always want to begin the time evolution with states $|\psi_E(T)\rangle$ that are reasonably well localized so that we can explore their subsequent spreading. For finite Γ, the state constructed by eq 5 will indeed by fairly well localized with our choice of $|\psi_0\rangle = \delta_{i,i_0}$. For E near the center of the band, the projection poses no problem because such extended states have reasonable overlap with $|\psi_0\rangle$. However, a localized state with E near the band edge might well be centered spatially about a site far from the origin i_0 and hence have a very small overlap with $|\psi_0\rangle$. To deal with this possibility we perform an initial projection with a broad state $|\psi_0\rangle$ which has equal amplitude on all sites. This initial projection results in a localized state about some site or sites in the lattice. The choice of one of these sites then serves to identify a new origin i_0. We the perform the usual projection with $|\psi_0\rangle = \delta_{i,i_0}$ with this new origin which has good overlap with the desired eigenstate and a controlled spatial extent.

In Figure 3a–d, we show values for the quantity $\langle \psi_E(T)|(\hat{H} - E)^2|\psi_E(T)\rangle$ as a function of T. The lattice size is 40^3, the initial state $|\psi_0\rangle$ is localized at the center of the cube, the energy $E = 0$, and $\sigma = 2$, 4, 8, 16, respectively. For our Hamiltonian, the energy eigenstates are roughly symmetric about the origin, so $E = 0$ corresponds to the band center. Similar curves are obtained for states of $E \neq 0$, even out to the band edge. It is seen that regardless of the choice the energy and static randomness, $\langle \psi_E(T)|(\hat{H} - E)^2|\psi_E(T)\rangle$ decreases by several orders of magnitude

(23) Barma, M.; Shastry, B. S. *Phys. Rev.* **1981**, *B18*, 3351.

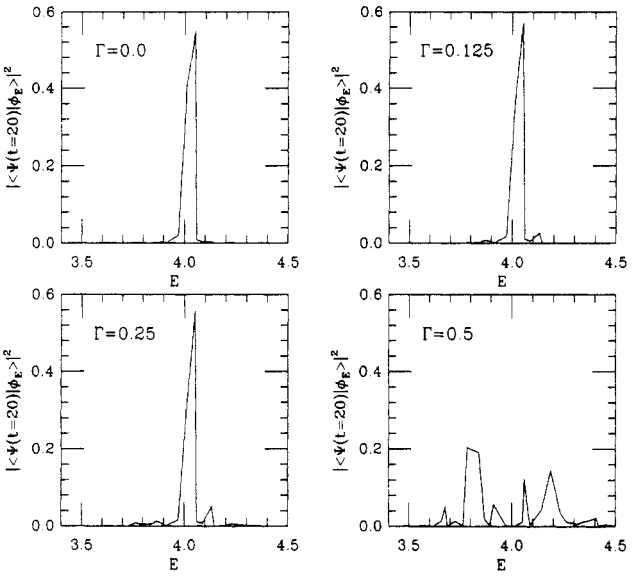

Figure 4. Plot of the spectrum of the state projected at $T = 20$ vs energy for an 8^3 lattice with V 1, $\sigma = 6$, and $dt = 0.025$. The panels show varying projection widths, Γ of 0.00, 0.125, 0.25, and 0.5.

by the time $T \approx 4$. On an 8^3 lattice we can diagonalize $\hat{H}$ exactly and look at the overlap of the projected state with the exact eigenstates. In Figure 4a–c we show such overlaps for $E = 4$, $\sigma = 2$, and $\Gamma = {}^1/_8$, ${}^1/_4$, and ${}^1/_2$.

As was alluded to earlier, the statement that the wave packet has energy E is strictly speaking a meaningful one only for $\eta = 0$. When the dephasing rate is nonzero, it is important to know how rapidly E evolves from its initial value. Figure 5a shows the energy E as a function of time for $\sigma = 6$ and $\eta = 0.0$, 0.5, 1.0, and 2.0 on a 40^3 lattice. Figure 5b shows the corresponding width of the energy of the wave packet for the same parameters. We see that, for small η, the time scale involved in shifting E is long relative to the time it takes to set the diffusion constant. Thus if we studied properties of the wave packet on time scales short compared to this, we would indeed obtain results characteristic of the initial energy. For longer time scales we obtain information about the evolution averaged over some range of energies. This may, in some situations, be the physically relevant case to study.

4. Results

In order to characterize the nature of the eigenstates and their transport properties we consider two quantities. The first is the "inverse participation ratio"[24]

$$\mathcal{P}^{-1} = \sum_i (\psi_i \psi_i^*)^2 \tag{6}$$

For a state localized on site i_0, ψ_i is roughly unity for $i = i_0$ and zero everywhere else. Thus $\mathcal{P} \approx 1$. On the other hand, for a delocalized state $\psi_i \approx 1/N^{1/2}$, where N is the number of sites. Then $\mathcal{P} \approx N$. Hence $\mathcal{P}$ is a measure of the number of sites participating in the state.

The second quantity we study is the diffusion constant. We find empirically that in the presence of nonzero σ and σ' that the mean square distance for the center of the box i_0

$$\langle x^2(t) \rangle = \sum_i (x_i - x_{i_0})^2 |\psi_i(t)|^2 \tag{7}$$

grows roughly linearly with time. For example, Figure 6 exhibits $\langle x^2(t) \rangle$ as a function of t for a typical case, $\sigma = 4$ and $\eta = 0$, 1, 3, 5. We can extract a diffusion constant D by defining

$$\langle x^2(t) \rangle = Dt \tag{8}$$

A third quantity of interest is the rate of decay of probability from a site as the state evolves in time. This is directly related

(24) Prelovšek, P. *Phys. Rev.* **1978**, *B18*, 3657. Thouless, D. J. *Phys. Rep.* **1974**, *13*, 93.

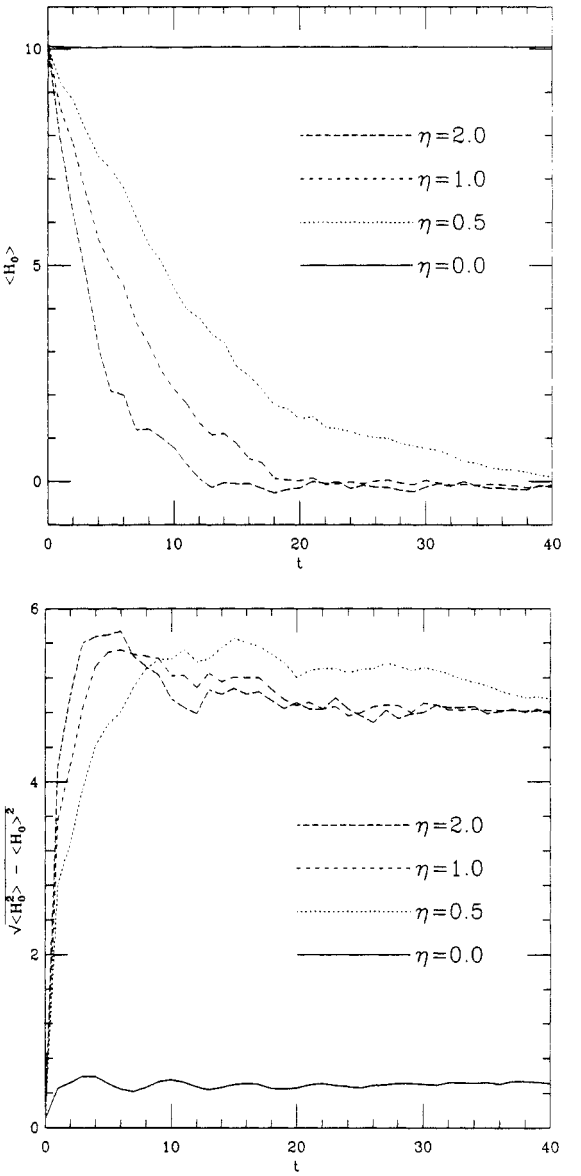

Figure 5. Plot of expectation value of energy of the system excluding the random time-dependent field, $\langle H_0 \rangle$ (a, top), and its standard deviation $(\langle H_0^2 \rangle - \langle H_0 \rangle^2)^{1/2}$ (b, bottom) vs t for a 20^3 lattice with $V = 1$, $\sigma = 6$, $dt = 0.025$, and $E = 10.0$. Each panel shows dephasing rates η of 0.0, 0.5, 1.0, and 2.0.

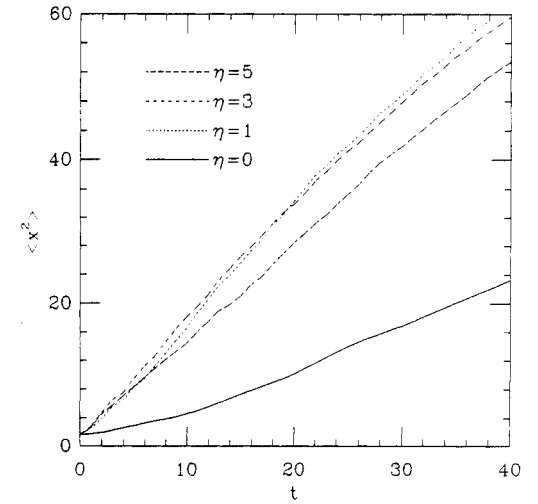

Figure 6. Plot of the expectation value of the square of the distance from the origin $\langle x^2 \rangle$ vs t for a 20^3 lattice with $V = 1$, $\sigma = 6$, $dt = 0.025$, and $E = 4.0$. The panels show dephasing rates η of 0.0, 1.0, 3.0, and 5.0.

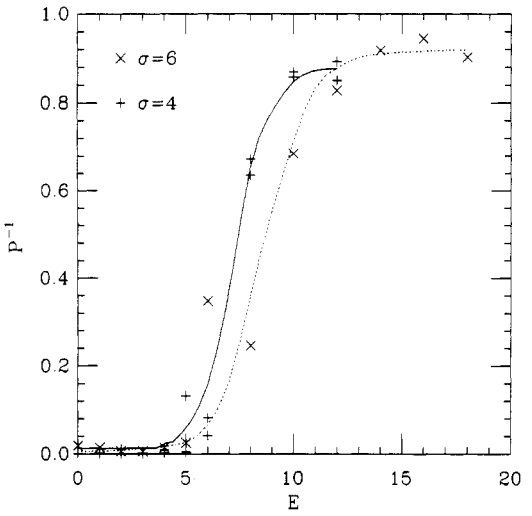

Figure 7. Plot of the inverse participation ratio vs target projection energy, E, for 40^3 lattice with $V = 1$, $dt = 0.025$, $\eta = 0.0$. Values are shown for static Gaussian randomness σ of 4 and 6. The curves are guides to the eye.

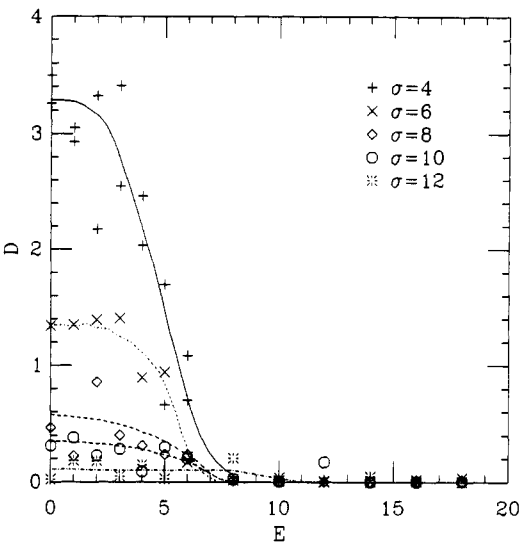

Figure 8. Plot of the diffusion constant, D, vs target projection energy, E, for 40^3 lattice with $V = 1$, $dt = 0.025$, $\eta = 0.0$. The evolution of the wave packet was done without dephasing. Static randomness shown has a Gaussian width σ of 4, 6, 8, and 10. The curves are guides to the eye.

to the imaginary part of the self-energy of the electron and is a quantity directly connected with the Logan–Wolynes theory. We will examine this decay rate in a later publication.

Let us begin by considering the problem without dephasing, i.e., $\eta = 0$. The interesting physics is to locate the mobility edge. In Figure 7 we show the inverse participation ratio for a state of energy E as a function of E for 40^3 lattices with $\sigma = 4$ and 6. A fairly sharp mobility edge is seen. We note that the bandwidth is increasing as we increase σ, so that in fact, as the static randomness is increased, the mobility edge when normalized to the bandwidth is moving in toward the band center. For $\sigma > 6$ fluctuations make the mobility edge determination difficult. In fact, states near the band center have fewer than 100 sites participating, so all states are essentially localized.

Despite extensive analytic and numeric work, there is some disagreement concerning both the precise numerical value for the critical amount of static randomness which localizes the entire band[25] and the mobility edge energy.[26-28] Values for σ_c for the Gaussian noise we consider here range from 4.8 to 8.7, with the preponderance of values at the latter extreme. While we have not attempted a precise determination of this value, our results are consistent with these larger values of σ_c.

We can also examine the diffusion constant $D(E)$ to locate the mobility edge. In Figure 8, $D(E)$ is plotted for the same values of (σ/t) as in Figure 7. Again a fairly sharp transition is seen at an E_c roughly consistent with that obtained in P^{-1}.

We next explore the effect of dephasing on the diffusion constant. In Figure 9 we show the diffusion constant as a function of η starting with energies $E = 0$, 6, and 14 with $\sigma = 6$. From Figure 7, we expect that the first two energies should correspond to delocalized states and the third to a localized one. Indeed, we see the expected qualitative behavior of the diffusion constant. For the delocalized states, increasing η from zero either monotonically inhibits the spreading of the wave packet or produces a weak maximum. For the localized states it first enhances and then inhibits spreading. This is in conformance with the mean field theory predictions of Logan and Wolynes.

For a localized state, the diffusion constant should depend linearly on η in the small η regime. Indeed, a fit of the $E = 14$ data yields $D(\eta) \approx \eta^{0.95\pm0.05}$. More precisely, the slope of $D(\eta)$ at $\eta = 0$ is just the inverse participation ratio, which has a value

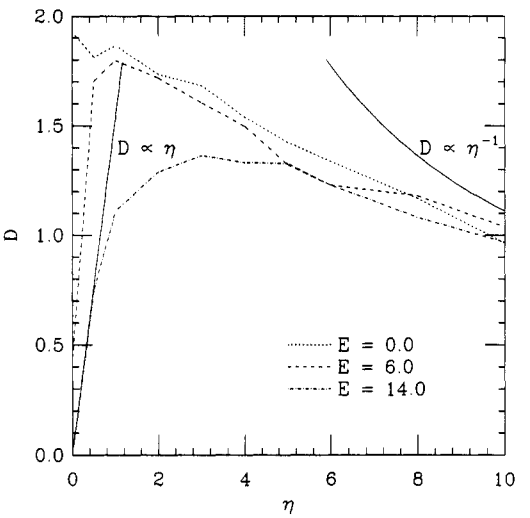

Figure 9. Plot of diffusion constant, D, vs dephasing rate, η, for a 20^3 lattice with $V = 1$, $dt = 0.025$, and a Gaussian width σ of 6 for the static randomness. Energies of 0, 6, 14 are shown. The initial wave function is a state that is localized about an initial site i_0 chosen from a projection as described in the text. The expected behaviors at large and small η for a localized state are also shown.

of order unity for a localized state. For delocalized states, P diverges with the size of the lattice and $D(\eta)$ comes into $\eta = 0$ with an infinite slope. We find that at the "critical point" (the mobility edge) $D(\eta) \approx \eta^{\alpha}$ with $\alpha = 0.57 \pm 0.02$. Meanwhile, for localized and delocalized states alike, the large η dependence is $D \approx 1/\eta$. The two limiting behaviors appropriate for localized states are shown also in Figure 8.

5. Conclusions

We have studied a model of the effects of dephasing on Anderson localization. We obtain a qualitative picture for the enhancement of transport by dephasing for states which are localized in the absence of dephasing ("phonon-assisted hopping") and an inhibition of transport for delocalized states. This is the usual Mooij correlation, i.e., the observation that for dirty metals with a high residual resistivity the temperature coefficient of resistivity is negative, while for clean metals with a low residual resistivity it is positive. For all cases, the diffusion constant for large η decreases as η^{-1}. This corresponds to the incoherent transport limit where the self-energy has an imaginary part which goes as V^2/η. The linear dependence of D on η for η small, characteristic of

(25) Kolley, E.; Kolley, W. *J. Phys.* **1988**, *C21*, 6099 and references contained therein.
(26) Bulka, B. R.; Kramer, B.; MacKinnon, A. *Z. Phys.* **1985**, *B60*, 13 and references contained therein.
(27) Schreiber, M. *Phys. Rev.* **1985**, *B31*, 6146.
(28) Economou, E. N. *Physica* **1984**, *127B*, 246.

localized states, is modified at the mobility edge where D now depends on η as a power law with exponent $\alpha \approx 0.57$.

Acknowledgment. P.G.W. very much would like to thank Harry Drickamer for being such a wonderful role model for those striving to combine chemical and physical modes of thought. D.A.E. and R.T.S. acknowledge useful conversations with Mark Friedrichs. This work was supported by NSF grant NSF-DMR 86-12860. Some of the computations were carried out at the National Center for Supercomputing Applications in Urbana, IL. We thank Karl Hess for providing time on his Ardent supercomputer.

Similarities and Differences in the C–C Bond Scission of Ethylene and Acetylene on Supported Ir and Pt Clusters

Po-Kang Wang,[†] Charles P. Slichter,*[,‡]

Department of Physics and Materials Research Laboratory, University of Illinois at Urbana-Champaign, Urbana, Illinois 61801

and John H. Sinfelt

Exxon Research and Engineering Company, Annandale, New Jersey 08801 *(Received: July 6, 1989)*

We have used NMR to study the C–C bond scission of adsorbed acetylene and ethylene on supported Pt and Ir clusters. We have monitored the extent of C–C bond scission by measuring the ^{13}C–^{13}C dipolar interaction. We have found that C–C bond scission of adsorbed ethylene has the same reaction path and activation energy (36 kcal/mol) on Pt and Ir. On the other hand, the predominant intermediate undergoing C–C scission in the case of adsorbed acetylene is different for the metals, and the activation energies are also different (37 kcal/mol on Ir and 53 kcal/mol on Pt). By measuring the ^{13}C–^{1}H dipolar interaction, we have found an extensive dehydrogenation of adsorbed acetylene prior to C–C bond scission on Pt clusters. The results are discussed in relation to Sinfelt's studies of the reaction kinetics of ethane hydrogenolysis and are shown to support the conclusions drawn by Sinfelt.

Introduction

One of the most interesting phenomena in catalysis is the drastically different abilities of different metals to catalyze particular reactions. For instance, the rate of ethane hydrogenolysis ($C_2H_6 + H_2 \rightarrow 2CH_4$) on Ir is about 6 orders of magnitude higher than that on Pt.[1] On the basis of the data of the reaction kinetics, Sinfelt concluded that the composition of the chemisorbed intermediate C_2H_x undergoing C–C bond scission depended on the metal.[1] By studying the temperature dependence of the reaction rate, he deduced barrier heights for breaking the C–C bond of 35, 36, and 54 kcal/mol for Os, Ir, and Pt, respectively. In this paper we report an NMR study of the C–C bond scission of adsorbed acetylene and ethylene on Pt and Ir clusters. (We include some data from acetylene on Os.) We contrast the similarities of the C–C bond scission of adsorbed ethylene on the two metals with the situation for acetylene in which the rate of C–C bond scission differs strongly between Ir and Pt. We show that the C–H bonds of the adsorbed acetylene break before scission on the C–C bond on Pt but not on Ir. We find that these results give a detailed confirmation of Sinfelt's earlier results on ethane hydrogenolysis by these metals. To set the present work in context, it is useful to keep in mind Sinfelt's work. For the various metals, he investigated how the rate of production of CH_4 depended on the temperature and on the partial pressures of C_2H_6 and H_2. He concluded that the hydrogenolysis rate was limited by C–C scission in a chemisorbed species C_2H_x.

We have previously determined the structure of adsorbed acetylene and ethylene on Pt, before and after C–C bond scission.[2-4] The structure is determined by the NMR measurement of ^{13}C–^{13}C and ^{13}C–^{1}H dipolar interactions and ^{13}C line shapes. We have found that, before C–C scission, the structure of adsorbed ethylene on Pt is CCH_3 (an ethylidyne species), the structure of the majority (about 3/4) of adsorbed acetylene on Pt is CCH_2, and the structure of the minority (about 1/4) is HCCH. Recently, our group[5] has used deuterium NMR to confirm the formation of CCH_3 from ethylene on Pt. After adsorbed ethylene or acetylene has been heated to 690 K, the C–C bond breaks and the remnants are mostly isolated carbon atoms, a small amount of methane, and hydrogen.[4] In this paper we study the processes and the activation energies of C–C bond scission of adsorbed acetylene and ethylene. We compare the reaction on Pt with that on Ir and discuss the relation of our results to those of Sinfelt for the ethane hydrogenolysis reaction.

Experimental Aspects

Our samples are small Pt, Os, or Ir clusters supported on η-alumina. The dispersions (percentage of metal atoms on the surface) are measured by hydrogen chemisorption. The dispersions of the Pt samples are 51% and 58%. The dispersion of the Os samples is 40%, and that of the Ir samples is 86%. The Pt and Ir samples are cleaned at 570 K under alternating flows of H_2 and O_2 gas and then evacuated to 10^{-6} Torr. The samples are cooled to room temperature under vacuum, ^{13}C-enriched ethylene or acetylene gas is admitted, and the samples are sealed off in glass vials. Typical sample size is about 1 cm^3. The ethylene coverages are 25% on Pt, 8% on Os, and 15% on Ir. The acetylene coverages are 25% and 50% on Pt, 28% on Os, and 25% on Ir. The low ethylene coverages on Os combined with its lower dispersion made studies of ethylene on Os substantially more difficult. Therefore, most of the data in this paper are concerned with Pt and Ir, though we report a bit for acetylene on Os.

[†] Present address: IBM Almaden Research Center, San Jose, CA 95120.
[‡] Also Department of Chemistry.

(1) Sinfelt, J. H. *J. Catal.* **1972**, *27*, 468; *Prog. Solid State Chem.* **1975**, *10*, 55.
(2) Wang, P.-K.; Slichter, C. P.; Sinfelt, J. H. *Phys. Rev. Lett.* **1984**, *53*, 83. Wang, P.-K. Ph.D. Thesis, University of Illinois, Urbana, IL, 1984.
(3) Wang, P.-K.; Slichter, C. P.; Sinfelt, J. H. *J. Phys. Chem.* **1985**, *89*, 3606.
(4) Wang, P.-K.; Ansermet, J-Ph.; Slichter, C. P.; Sinfelt, J. H. *Phys. Rev. Lett.* **1985**, *55*, 2733.
(5) Zax, D. B.; Klug, C. A.; Slichter, C. P.; Sinfelt, J. H. *J. Phys. Chem.* **1989**, *93*, 5009.

0022-3654/90/2094-1154$02.50/0